DYNAMIC MODELLING AND VALIDATION OF THE METAL/FLUX INTERFACE IN CONTINUOUS CASTING

K.Pericleous[1], G.Djambazov[1], JF. Domgin[2], P. Gardin[2]
[1]Centre for Numerical Modelling and Process Analysis
University of Greenwich, London, UK
[2]ArcelorMittal,
Maizieres-les-Metz, France

Abstract

This paper concerns the development and validation (using an oil/water system) of a finite volume computer model of the continuous casting process for steel flat products. The emphasis is on hydrodynamic aspects and in particular the dynamic behaviour of the metal/slag interface due to the momentum imparted by the submerged entry nozzle (SEN) jets that bring the metal into the mould. Instability and wave action encourage the entrainment of inclusions into the melt affecting product quality. To track the interface between oil and water a new implicit algorithm was developed, called the Counter Diffusion Method. To prevent numerical damping of low frequency waves, a time-filtered version of the k-ε model was incorporated in the model. The physics of the interface dynamics are affected by density stratification and surface interfacial tension, with additional source terms introduced in the turbulence model to account for the former effect. Gas bubbles were modelled using a Lagrangian tracking method. The model was validated against experimental measurements obtained in a water model apparatus at Arcelor Research. Silicon oil was used to represent the lighter layer whilst air was pumped through the SEN to represent the argon.

Keywords: continuous casting, interfaces, turbulence modelling

1 Introduction

This research is part of a continuing programme that concerns the development of a complete model of the mould region of the continuous caster for steel plate products. The programme of research encompasses (a) fluid dynamics aspects and slag/metal interface motion, (b) heat transfer and solidification, (c) mass transfer and chemical reaction at the slag/metal interface. This contribution reports work on part (a), concentrating on fluid dynamics in the mould region, with particular emphasis of the dynamic aspects of the interface and the effects of turbulence.

The flow development is governed by the action of the Submerged Entry Nozzle (SEN) jets that deliver the metal from the tundish to the mould. Due to its importance in final product quality, the flow in this region is a subject of considerable interest in the research community (e.g. see Thomas [1]). The flowfield is important as it determines the heat transfer in this region and the initial formation of the plate shell. The twin SEN jets, direct hot metal towards the long ends of the plate and once they reach the mould wall they are quenched first by contact with the water-cooled copper mould surface and further downstream by water cooling sprays. The Reynolds numbers involved are such that the flow in this top region is invariably turbulent which again has a considerable influence on how heat is distributed in the melt. As it is shown by water model experiments [2] and other numerical simulations [3,4,5], the jets are diverted at the wall to form two recirculation loops, a deep loop in the casting direction and a short upper loop which returns flow along the flux metal interface towards the SEN wall. Control of these loops is important in the continuous casting process as it determines the transport of inclusions (oxide impurities, gas bubbles, slag droplets) into the solidifying skin leading to defects.

To prevent nozzle clogging, argon gas is injected into the SEN together with the liquid metal and the presence of the resulting gas bubbles leads to additional effects: bubbles add buoyancy to the jets altering the upper jet loop, they encourage mixing of the slag with the steel at the interface, and also act as inclusion carriers. The flow computation needs to account for these bubbles, the result being a three-phase calculation [4] with a moving interface.

The slag metal interface itself has a dynamic character since the 1:4 density ratio across it encourages the development of gravity waves. These waves are present even with a stationary mould and they appear to be excited by the SEN jets and also by the presence of gas bubbles [4]. Interface shear then leads to the break up of molten flux droplets through a Kelvin-Helmholtz instability mechanism (e.g. see Iguchi et al.[6]). Water/oil experiments show [2] that the behaviour of the interface depends on both gas and liquid flow rate, and suggest that large water flow rates may uncover part of the steel surface, close to the narrow ends of the mould. The experiments also suggest that SEN jet momentum is reduced as gas flow rate increases and mixing at the slag metal interface becomes more vigorous.

In this paper an attempt is made to capture these complex effects in a single multi-physics simulation. The water/oil LDA and video capture experiments at Arcelor Research are used to validate the computer model.

2 Experimental Setup

2.1 The Water Model

Data were obtained in an experimental water model rig (see Figure 1). The experimental rig has an adaptable geometry which allows the testing of different mould dimensions and various SEN designs. Both mould and SEN are transparent and they are located in a robust support. Water circulation is provided by a pump that draws water from the collector at the bottom of the mould and pushes it into a reservoir, the tundish, located at the top of the mould. Different flow rates can be easily selected and the system is also provided with electronic control for the immersion depth of the SEN. Measurements are taken using the LDA technique.

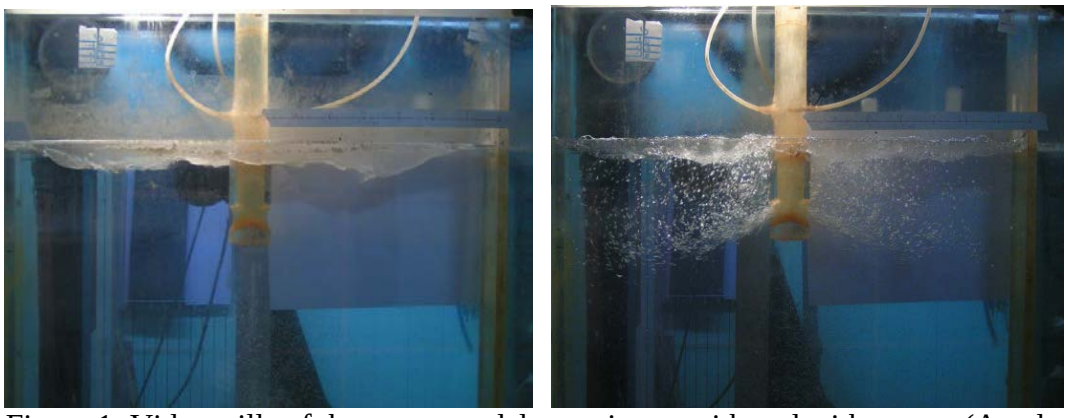

Figure 1: Video stills of the water-model experiment with and without gas (Arcelor Research, 2005 [2])

In the experiment silicon oil was used to mimic the slag layer and air was pumped through the SEN to mimic argon gas. Data were then collected for different water and gas flow rates and for different oil layer thicknesses. Horizontal velocity and its distribution in time were monitored in 15 experimental points along the middle plane of the mould as shown schematically in Figure 2.

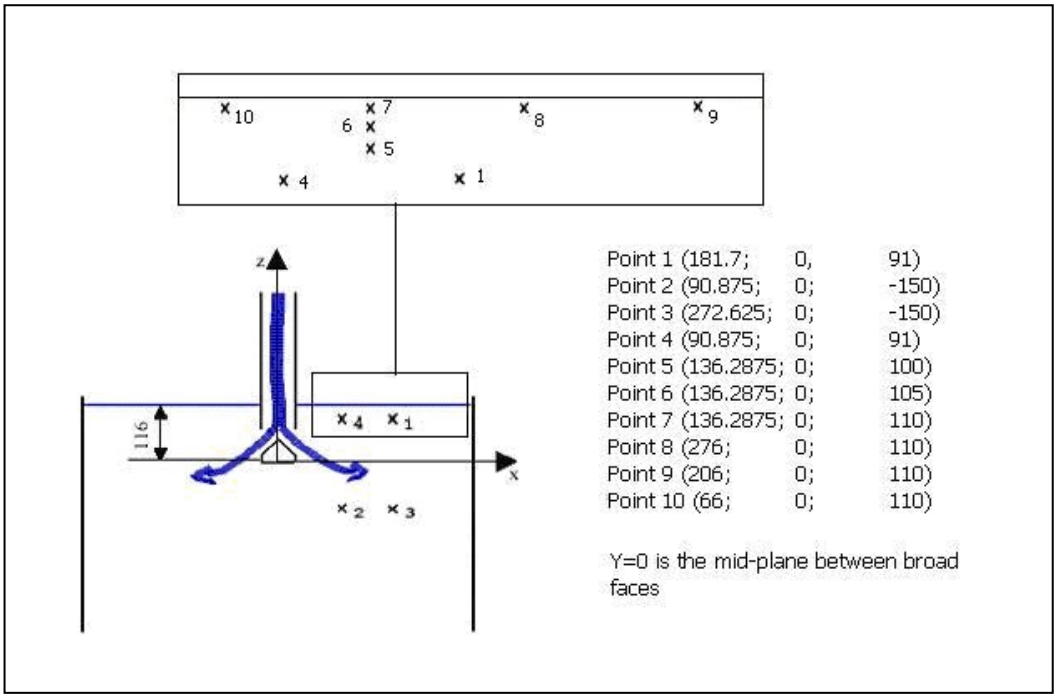

Figure 2: LDA measurement points

2.2 Data Analysis

With the setup just described, experimental data were collected at the specific points, shown in Figure 2. Of the 10 points displayed, only numbers 1-5 were usable, as the others were too close to the moving interface to be reliable.

In order to compare the experimental data against simulations a certain amount of manipulation was necessary: (1) The data had to be filtered to remove high frequency spikes which are unlikely to have a hydrodynamic source, (2) averaged to determine the mean value of the signal and then (3) the average subtracted before a spectral analysis could be carried out.

Figure 3 shows the difference between the filtered and raw LDA signals. The raw signals exhibit peaks of 1m/s but with duration of 1ms or less, unlikely for a fluid with inertia, so these signals were excluded from subsequent frequency analysis by the filtering process. Various filter sizes were tested and the filtered signal with a base of 2s is shown in the right-hand part of Figure 3.

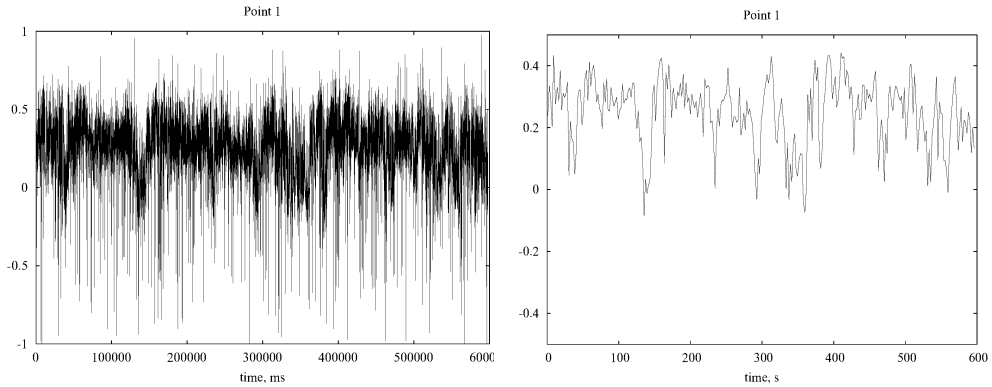

Figure 3: Comparison of raw and filtered signals from Point 1 with a filter base of 2s

The finite volume method is used to discretise the governing equations in an unstructured centre-collocated scheme and the resulting linear system of equations is solved iteratively within the home-grown code PHYSICA [7]. The equations used are described in the remainder of this section.

3. **Mathematical Model**

The simulation of the casting process models the continuum as a mixture of liquid/solid metal, molten flux and argon bubbles. In this three-phase simulation a Lagrangian particle-tracking algorithm is used to predict the motion of the argon bubbles. Coupling between the mean flow and the bubbles is achieved through density variations in elements containing argon. Phase change within the metal is modelled through an enthalpy source-based method. The position of the interface between the metal and the molten flux is computed using an implicit VOF-type method, optimized for speed using a counter-diffusion interface sharpening algorithm. The resulting flowfield is turbulent with turbulence represented via an effective viscosity derived from a k-ε model formulation. The k-ε model is itself filtered to account for the time stepping nature of the calculation as explained below.

3.1 Momentum and Continuity

The conservation equations for momentum and mass for three dimensional fluid flow expressed in vector notation are

$$\frac{\partial}{\partial t}(\rho \underline{u}) + \nabla.(\rho \underline{u}\underline{u}) = \nabla.(\mu \nabla \underline{u}) - \nabla p + \underline{S} \quad (1)$$

$$\frac{\partial \rho}{\partial t} + \nabla.(\rho \underline{u}) = 0 \quad (2)$$

where $\underline{u}$ the velocity vector, p is the pressure, ρ is the mixture density and μ is the effective viscosity (sum of laminar and turbulent contributions). The turbulent viscosity is calculated through the solution of a standard k-ε model. The source vector in the momentum equation, $\underline{S}$, includes the body forces, such as buoyancy, boundary effects and for solidification problems the Darcy source. The Darcy source represents the resistance to flow resulting from the presence of solid and is equal to

$$\underline{S} = \frac{\mu}{K}\underline{u} \qquad (3)$$

where K is the permeability calculated here using the Carmen-Kozeny equation

$$K = \frac{f_L^3}{\zeta(1-f_L)^2} \qquad (4)$$

where f_L is the fraction of liquid as a function of temperature T, and ζ is constant associated with the mushy region.

3.2 Heat Transfer and Solidification

The energy equation, with temperature as the dependent variable, is given by

$$\frac{\partial}{\partial t}\left(\rho c_p T\right) + \nabla.\left(\rho c_p \underline{u} T\right) = \nabla.\left(k\nabla T\right) + S_T \qquad (5)$$

where k is the thermal conductivity and c_p is the specific heat. The source term, S_T, contains the contributions from the boundaries and the effects of phase change. The energy released due to a change of phase can be expressed as

$$S_T = -\frac{\partial}{\partial t}\left(\varphi\rho_m f_L L\right) - \nabla.\left(\varphi\rho_m \underline{u} f_L L\right) \qquad (6)$$

where L is the latent heat of solidification, ρ_m is the density of the metal and ϕ is the fraction of metal obtained from the free surface model. A linear liquid fraction variation was chosen in the mushy zone between the solidus T_S and liquidus T_L temperatures as shown in equation (7):

$$f_L = f_L(T) = \begin{Bmatrix} 0 \text{ for } T < T_S \\ (T - T_S) \big/ (T_L - T_S) \\ 1 \text{ for } T > T_L \end{Bmatrix} \qquad (7)$$

3.3 The Free Surface Model

The interface between the molten flux and the liquid metal is modelled using the scalar equation algorithm [4]. The algorithm solves the equation

$$\frac{\partial \varphi}{\partial t} + \underline{u}.\nabla \varphi = 0 \qquad (8)$$

for the metal volume fraction in an element, ϕ, on a stationary mesh. The continuity equation (2) is reformulated to represent volume conservation

$$\frac{D(\ln \rho)}{Dt} + \nabla.(\underline{u}) = 0 \qquad (9)$$

where *D/Dt* is the substantial derivative of density. Since then, density gradients are represented by their logarithm, numerical accuracy is improved close to the interface.

3.3.1 The Counter_Diffusion_Method for free surface tracking

The main practical problem in following a moving interface through a fixed mesh is that of maintaining a sharp property discontinuity. This is accomplished in the various traditional methods using specialised numerical schemes such as the Van Leer TDV scheme [8], the Level Set Method [9], or alternatively relying on a front sharpening/reconstruction scheme such as Donor-Acceptor [11]. However, all these schemes are explicit, which means time-steps have to be small enough to satisfy the CFL criterion. This criterion is based on the residence time of the flow in any particular cell, which can be prohibitively small in fine mesh regions needed to characterise the relatively small instantaneous deformation of the slag/metal interface. Exceeding the CFL limit, generally leads to numerical instability and diverged solutions. To avoid this hurdle, and speed up the computation time a new time-implicit method for tracking the free surface was developed and implemented, the CDM (Counter_Diffusion_Method) [10]. This method can lead to dramatic improvements, since much larger time steps (by an order of magnitude) can be employed. As the name implies, the interface is allowed to diffuse, but then this diffusion is countered by gathering the spread back in towards the interface. The main concept behind can be explained with reference to an air-water interface. Taking the interface to be at ϕ=0.5, any intermediate values of ϕ, $(0 < \phi < 1)$ can be interpreted physically to signify the presence of either droplets $(0 < \phi < 0.5)$ or bubbles $(0.5 < \phi < 1)$. As during gravity separation, droplets re-join the liquid and bubbles re-join the gas. This ‘sifting’ can be achieved by prescribing a suitable slip velocity to separate real bubbles or droplets. The process is similar to diffusion, but operating against the scalar gradient, hence the term counter-diffusion. A counter diffusion 'flux' is computed for each internal cell face when the face belongs to an interface cell. The relevant flux is:

$$flux = C\left|R_{fvel}\right|\left(1-\varphi_{dn}\right)\varphi_{up} \qquad (10)$$

Where C (= 4/3) is a scaling factor, R_{fvel} is the face-normal area velocity product, ϕ_{dn} and ϕ_{up} are downwind and upwind values of ϕ. With this formulation 'droplets' are pushed artificially back towards the liquid region; any gas in the liquid (bubbles) is then displaced automatically in the opposite direction by conservation. The factor (1-ϕ_{dn}) prevents sifting into completely full cells whilst ϕ_{up} ensures droplets are not taken from cells without liquid. The advantage of this method is that it can be used with any numerical scheme, and it can be implemented in both implicit and explicit formulations removing the strict CFL constraint.

CDM is still being evaluated, further developed and tested. Initial validation was carried out by comparison with the experimental study of a collapsing water column by J. C. Martin and W. J. Moyce [12]. The positions of the water front and the residual of the water column are plotted (in non-dimensional coordinates) as functions of elapsed time and compared with the experimental data in Figure 4 and Figure 5.

It can be seen that there is very good agreement between the numerical results and the experimental data. Although in Figure 4, the result with LSM is slightly less precise compared to the other methods, the general trends by the experimental data are obviously captured by all methods. From our perspective, more importantly comparisons of CDM can be seen from the point of view of efficiency as presented in Table1.

Table1. Comparisons of the efficiency of CDM with other numerical methods

Method	Δt_1 =0.1s		Δt_1 =0.05s		Δt_1 =0.01s	
	N	*t(s)*	*N*	*t(s)*	*N*	*t(s)*
Van Leer	divergence		Breaking CFL		10	47
Donor Acceptor	divergence		Breaking CFL		40	**132**
Level set	divergence		Breaking CFL		20	121
Counter Diffusion	20	**16**	15	17	5	34

Note: Δt =Timestep; *t*= Running time; *N*= average number of iterations per time step

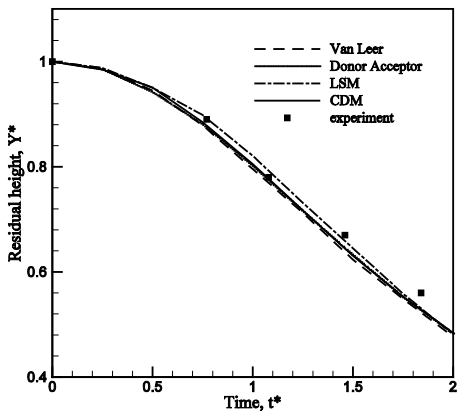

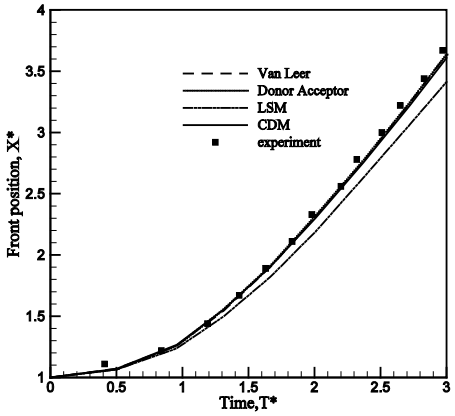

Figure 4. Comparisons of the numerical results with experimental results for the front position of the collapsing water column (Martin & Moyce 1952) [10]

Figure 5. Comparisons of the numerical results with experimental results for the residual height of the collapsing water column (Martin & Moyce in 1952)[10]

It can be seen that CDM, being implicit, can be applied with a bigger time step (CFL>1). Also, for the same time step, the number of iterations needed per time step is lower than that required by the other tracking methods. The first two columns show that the time step for CDM could be ten times bigger than the others and running time with Δt =0.1s is half that with a time step Δt =0.01s since more iterations within a time step are then needed. Nevertheless, even with the same small time step as the others, the number of iterations within CDM is largely lower, seen in the last two columns.
The total running time with Van Leer is at least double that with CDM for the same time step and with the most popular Donor Acceptor method it is almost four times that of CDM. Finally, comparing the best possible time obtained with CDM, 16s and Donor-Acceptor, 132s for the same results, gives an impressive gain of a factor of 8.25!

3.4 Turbulence Model & Modifications

Turbulence has an important role to play in these simulations, not just for its effect on the flowfield, but for its role in heat transport to the solidifying shell and to the flux layer. The current trend for simulating turbulence in continuous casting is by using the LES method [1,3]. However, this would lead to an increase in computational cost, so although LES models exist in PHYSICA, the standard k-ε model was adapted instead to our aim. It was observed both in our computations and in previous CFD computations performed by Arcelor, that although surface oscillations were successfully predicted in air, the presence of an oil layer led to their almost complete suppression in contrast to experiments. The turbulence model

was suspected for this behaviour. Two avenues were open to investigation: (1) The suitability of the k-ε model in transient simulations, (2) The effect of density change and interfacial energy on sub-grid turbulence at the interface.

The standard k-ε model is the one most widely used in many applications but it was created to describe steady state problems. Its use in transient problems is acceptable, provided the timestep used in the CFD simulation is not in the inertially important range of flow-induced eddies. Should that be the case, turbulent energy is overestimated leading to excessive diffusion. This would suppress the energy governing surface oscillations, so leading to artificial damping. To overcome this deficiency and fill the gap between LES and standard RANS models, a 'filter' in the Kolmogorov-Prandtl equation has been introduced to reduce the effective viscosity (Johansen [13]).

In general, when conducting fluid flow computations, it is desirable that the cell Reynolds number is not larger than O(1) so that the flow structure can be satisfactorily resolved. If the eddy viscosity is excessive it will smear out the flow structures that are within the reach of a given grid resolution. Imposing a filter implies that all the turbulence structures smaller than filter size will not be resolved. The filter size is chosen in according to the following expression

$$f_\mu = Min\left(1, C\frac{\Delta.\varepsilon}{k^{3/2}}\right);\ C \approx 1.0 \qquad (11)$$

Then, the turbulent viscosity is given by:

$$\mu_t = C_\mu f_\mu \rho \frac{k^2}{\varepsilon} \qquad (12)$$

Δ is the filter size, which is related to the characteristic length of the problem, that is to the shear layers generating the turbulent structures in the flow. With increasing filter size the 'filtered k-ε' model approaches the standard one. An advised filter size for symmetric wake flow is 0.075 *L*, where *L* is a characteristic length. This was determined by Johansen [13], by comparing the vortex street behind a square obstacle with experimental measurements. The model constant *C~1.0,* corresponds to the Smagorinsky constant in the original LES formulation.

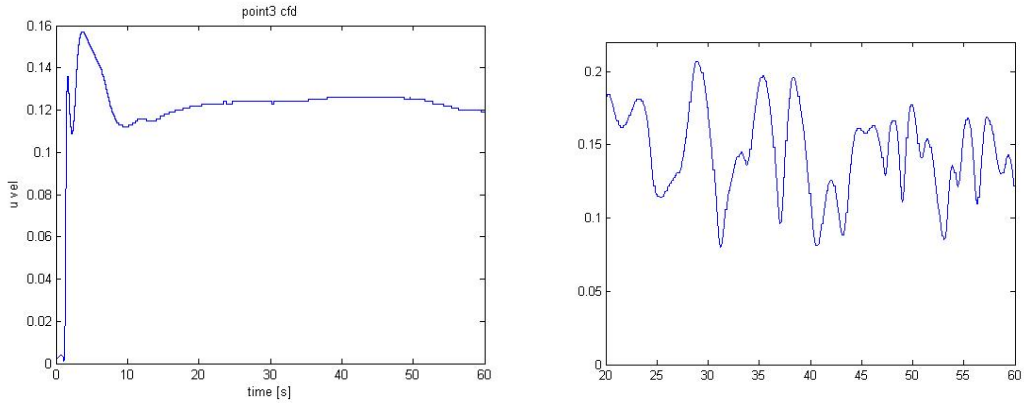

Figure 6: Horizontal velocity distribution point 3 (276,2.25,200) (simulation with 1cm oil, inlet velocity 1 m/s) showing the drastic effect of turbulence damping on oscillation amplitude

This adaptation of the k-ε model was implemented in PHYSICA for the continuous casting problem. The new version led to a significant change in the amplitude of surface oscillations and gave results that are more in accordance with experimental data, especially in the cases with an oil layer. Figure 6 shows the effect of the filter on the time variation of horizontal velocity for measurement Point 3, which lies in the path of the jet (see Figure 2). After an initial transient, the standard formulation prevents any oscillations persisting beyond the 10s mark. In contrast, the oscillation settles at ~5cm/s when the filter is applied. It is evident, that excessive turbulence diffusion is responsible for the damping.

The filter value chosen for the simulation is related to the size of the SEN port diameter. The exact value used is a matter of experimentation, although the Prandtl Mixing Length value for a round jet was considered a good start. Figure 7 shows the effect of two different filter lengths (3mm, 4.5mm) on the amplitude of oscillation at various experimental positions. The smaller filter size leads to larger amplitude, although the signal shape and frequency is not significantly altered. Although not explicitly stated in Johansen's papers, filter size and timestep are related, since the period of oscillation is related to wavelength.

The timestep effect can be seen in Figure 8 for two different values, 10ms and 20ms. Doubling the size of the timestep has an effect on the signal, in particular introducing a phase shift, which becomes apparent as time increases. The effect is most pronounced for Point 5, which is closest to the oil/water interface. It is obvious that the results at this stage are not timestep or filter independent. However, further validation is in progress, with values chosen as a compromise between accuracy and computational efficiency.

At the interface itself, there is another mechanism in action, affecting turbulent fluctuations, especially in the vertical direction. Interfacial tension acts to balance hydrostatic equilibrium, not only for the resolved interface deformation, but also for the unseen sub-grid deformations caused by turbulence. As shown by Iguchi et al.[6] the kinetic energy of turbulence is balanced, by changes in potential and interfacial energy through the expression,

$$V_1^2 - V_2^2 = \frac{\rho_1 + \rho_2}{\rho_1 \rho_2}\left((\rho_2 - \rho_1)\frac{g}{K} + \sigma_{12} K \right) \qquad (13)$$

Equation (13), is a consequence of the Kelvin-Helmholz instability theory with K being the wave number and σ_{12} the interfacial tension between phases *1* and *2*.

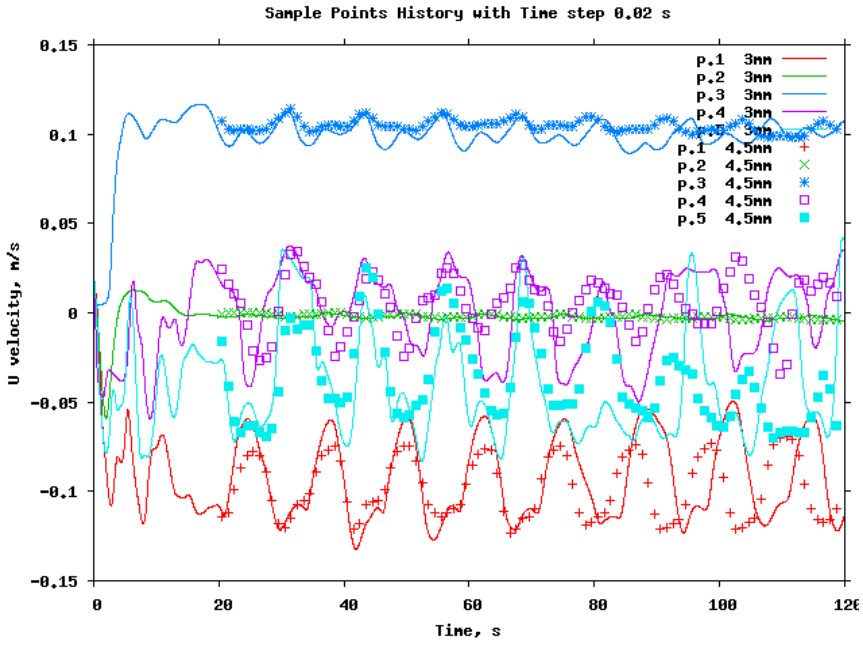

Figure 7: Effect of k-ε **filter size** on sub-surface velocity fluctuations (3mm & 4.5 mm filters)

In this implementation only the first term on the RHS of (13) was implemented being dominant at the frequency range of interest. In effect this term acts as a sink of turbulence in zones where the gradient of density is high (buoyancy stratification of turbulence). Physically, the vertical component of turbulent kinetic energy k_z is reduced between the two fluids since any displacement in the z, or diminishing density direction will lead to a restoring buoyancy force. Studies in the literature [14] show that the energy lost is returned to the directions parallel to the interface. So, the energy lost needs to be re-distributed in the other two kinetic energy components, k_y and k_x. Focusing only on the fluid dynamics of the problem we can neglect this detail, but it is thought it may be an important factor in heat transfer at the interface as the turbulent kinetic energy influences the heat exchange coefficient. Figure 9 shows the effects of the buoyancy stratification of the turbulence combined with the effect of the filter on turbulence viscosity. The filter takes away turbulent energy that has already been accounted for in the NS equations, hence the overall level is reduced. Then, the buoyancy stratification effect produces damping of turbulence at the oil/water interface which can be seen in the top of the right-hand figure. Elsewhere, turbulence levels are predicted to be high in the jet shear zone, in the vicinity of the narrow wall where the jet splits into upper and lower recirculation loops and in the wake region below the SEN.

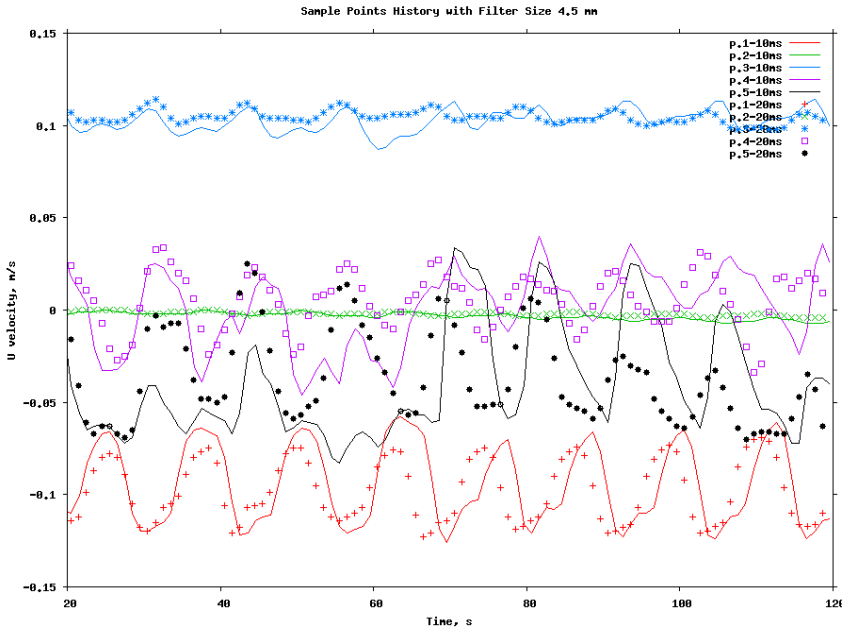

Figure 8: Effect of **timestep** size on sub-surface velocity oscillations. Filter size 4.5mm, δt = 10ms & 20ms

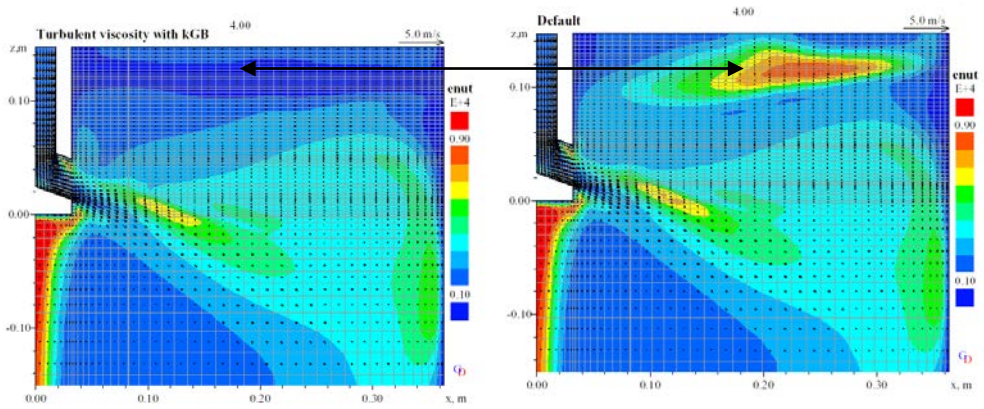

Figure 9: Contours of turbulent viscosity: Left with buoyancy stratification plus filter; right, filtered k-ε only

The implementation is analogous to that employed in fire modelling studies [15]. The buoyancy "stratification" term is implemented through a sink term in the k and ε equations, which is proportional to the density gradient in the gravity direction.

3.5 Particle Tracking Scheme

The particle-tracking model has some novel features [16], used to couple the particles to the mean flow through variation in the density field. The argon flow rate

is split into a number of parcels each carrying an equal mass such that the total mass equals the required inflow. One particle is tracked for each parcel using a conventional Lagrangian method. The particle velocity, U_p, is computed from

$$U_p = (U_p + S_u * \delta t)/(1 + F * \delta t) \tag{14}$$

Where

$$F = 0.75 * C_d * \rho * V_{slip} / (d_p \rho_p), \quad S_u = F * U_p + (\rho_p - \rho) * g / \rho_p$$
$$\text{and} \qquad V_{slip} = U_p - U \tag{15}$$

The subscript p indicates particle values, other values are those associated with the liquid metal or flux, d_p is the diameter of the particle and g the gravity constant. The particle time step size, δt, is chosen so that a particle takes a specified number of steps to cross an element. Two methods were used to calculate the drag coefficient C_d depending on the size of the bubble, the Reynolds number and the Weber number. Details are given in [16]. The particles are randomly seeded just inside the circular SEN inlet. Particles are assigned an initial velocity close to the continuum velocity, and tracked until they reach the metal-flux interface or solid metal. The time a particle spends in an element, Δt, is recorded and the argon volume fraction of the element is increased by

$$\Delta t (\dot{m}_{ar} / N_p) / \rho_p \tag{16}$$

where $\dot{m}_{ar}$ is the mass flow rate of argon at the inlet and N_P is the number of packets.

3.5.1 Effect of Turbulence on Bubbles

The effect of turbulence on particles is simulated using the stochastic model of Gosman and Ioannides [17], in which particles are deflected by the eddies they cross, and the continuous phase velocity U used in the drag term of particle momentum (14) is treated as the sum of the average velocity obtained from the momentum transport equation and a fluctuating component u' computed from the kinetic energy of turbulence, k. The effect on bubble dispersion is seen in Figure 10, where there is a clear spreading of the bubble tracks especially at smaller diameters.

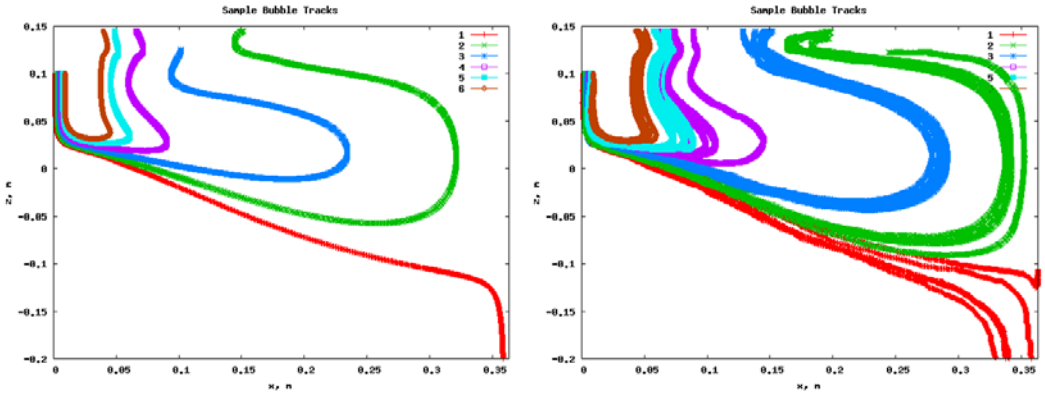

Figure 10 Effect of turbulence on bubble dispersion for 6 bubble groups, d=1-6mm

3.5.2 Bubbles at the Interface

At the approach to the interface, bubbles have to overcome the resistance imposed by the film generated between the two continuum fluids and the interpenetrating gas bubble (see Figure 11). The film drainage process introduces a delay which needs to be accounted for. In the oil/water experiments this delay seems to be very small. However, the case may not be so in a slag/metal system as shown by Chevrier [18]. This delay has not been introduced into the model yet, although bubbles are allowed to traverse the interface.

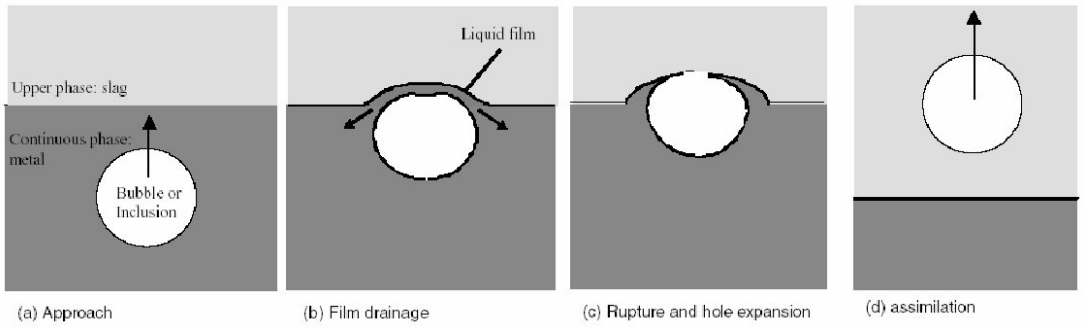

Figure 11 Schematic of a gas bubble approaching a metal/slag interface (reproduced from Chevrier & Cramb [18])

4. Computed Results

Several cases were studied, in particular to validate the model against water/oil experiments. Parameters considered include the oil layer thickness, casting speed (alternatively the SEN fluid velocity) and nozzle geometry. Some examples are given below.

Figure 12 compares a high flow rate case with 2cm oil cover, but no gas. The experiment on the right, clearly demonstrates that the oil layer is pushed away from the side wall of the mould by the upper recirculation jet, leaving the water surface uncovered. At the same time, the oil is dragged into the water with the layer thickening and some instability appearing at the interface between them. The simulation shows a similar result, although there are differences in the actual profile. Increasing the oil layer thickness as in Figure 13 leads to the surface being recovered, but there is still evidence of shear induced break up of the interface due to the top jet action.

The flow pattern developed is shown in a quarter-section computation of an actual caster in Figure 14. The light liquid is now slag produced by the melting of liquid powder and the heavy liquid is steel. The upper and lower recirculation loops are

clearly evident, plus the complex three dimensional nature of the flow in the upper part of the mould.

Figure 15 shows a water model simulation with a SEN with rectangular outlets. Time dependent simulations identify vortices at the oil-water interface, which appear to pull the lighter liquid, oil, into the water. The position of these vortices varies in time and can only be captured in a fine mesh simulation. Similar vortices appear in experiments.

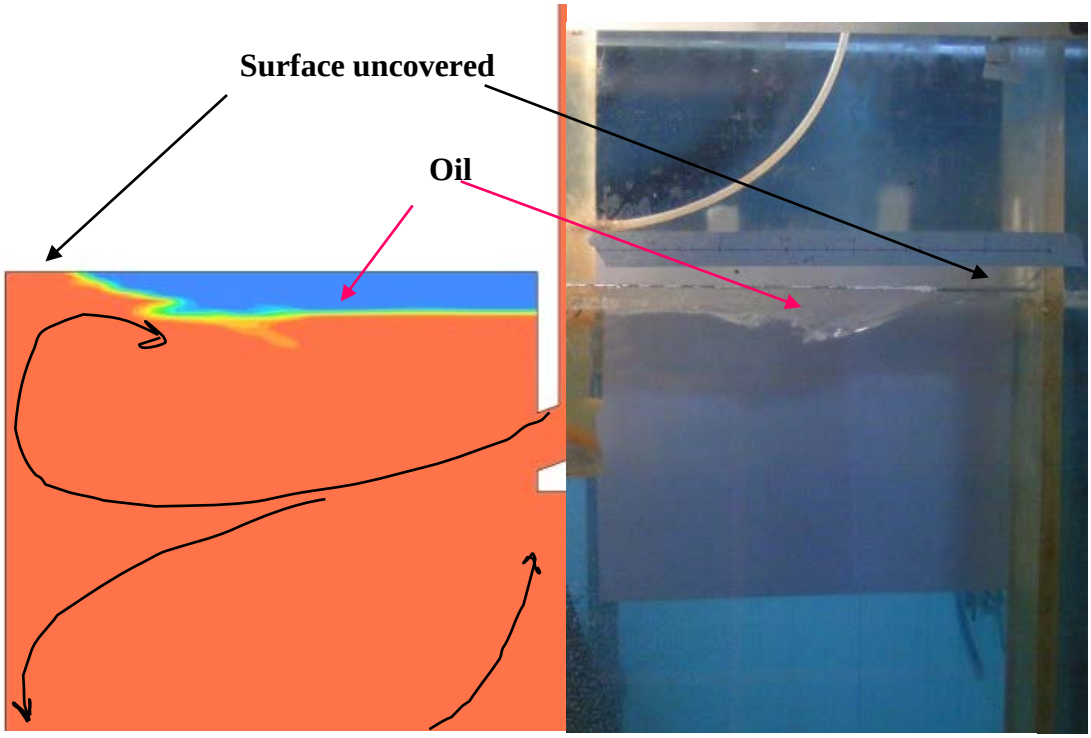

Figure 12: The case with a 2cm silicon oil layer. The simulation displays the same characteristics as the experiment, including the formation of folds and the uncovering of the narrow end of the water surface

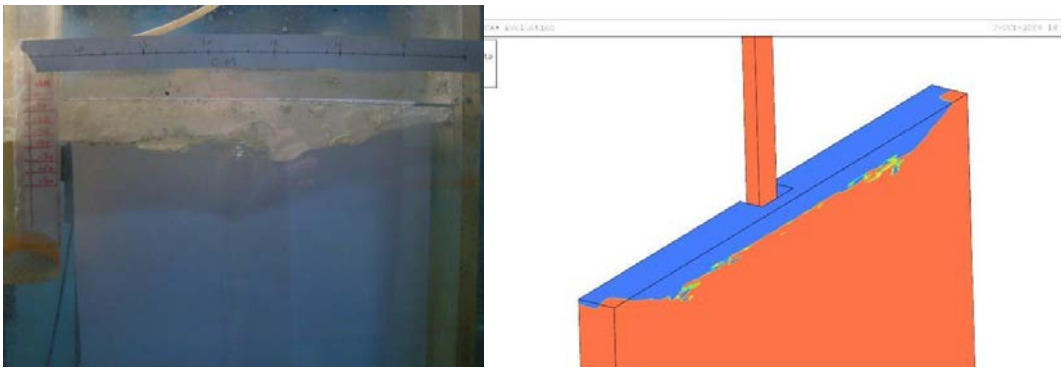

Figure 13: The water model case with a 3cm oil layer covering

Figure 16, shows the behaviour of bubbles as they enter the mould. The plots show contours of gas volume fraction and this simulation relates to a case without an oil layer on the surface. The Lagrangian model allows a mixture of bubble sizes to be prescribed, but no account is taken of coalescence or breakup at present. The plot shows some of the gas escaping straight to the surface on exit from the nozzle. This corresponds to the large bubbles, where buoyancy forces are dominant. Since the bubbles effectively change the volumetric density of the mixture, the SEN jets become shorter due to a reduction in momentum and also become more buoyant.

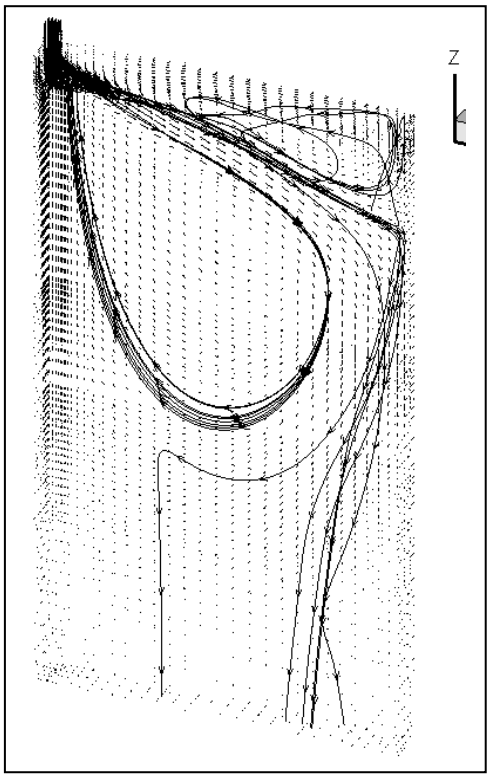

Figure 14 depicts in perspective one quarter of the mould section, and clearly shows the upper and lower convection loops formed once the SEN jet reaches the narrow section wall.

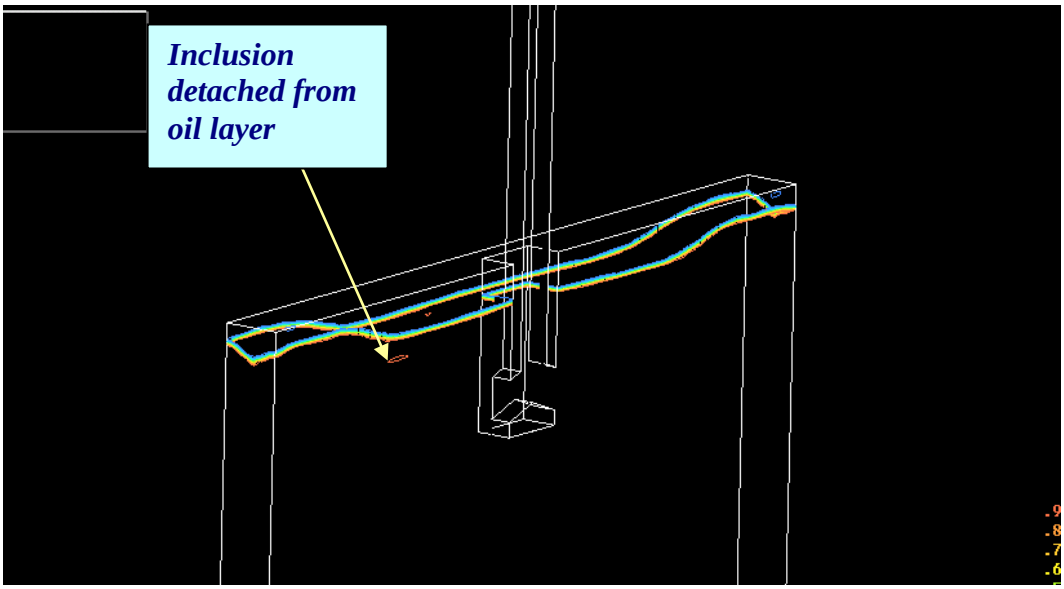

Figure 15 Time dependent calculations indicate the presence of vortices which drag the lighter phase as droplets into the heavy phase.

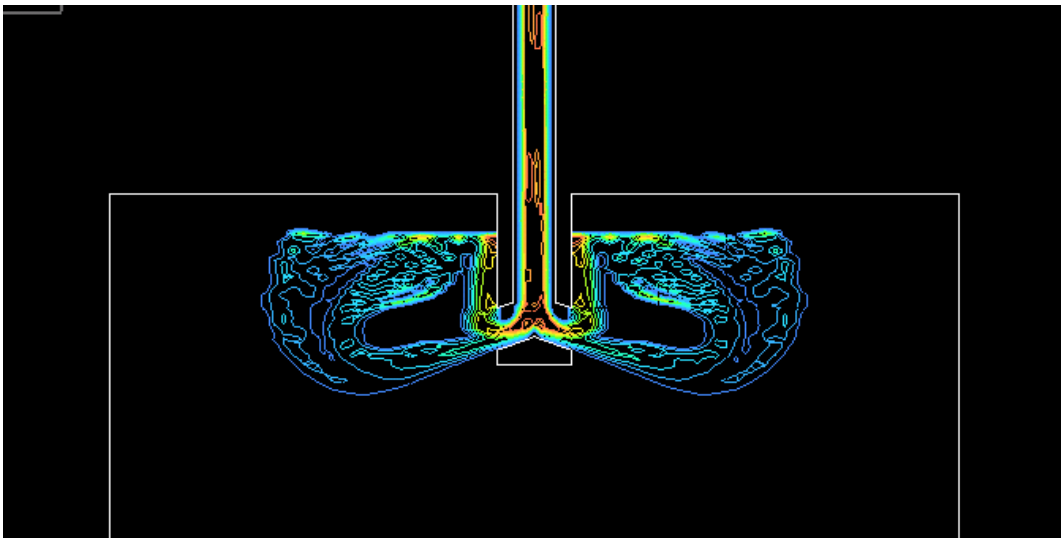

Figure16: Gas concentration obtained for the case without an oil layer cover

When an oil layer is added, then the question arises as to how the bubbles penetrate the surface, the delay imposed by interfacial tension to allow for film drainage and the amount of heavier fluid entrained in their path. Figure 17 illustrates this effect for two specific particle size streams, for diameters of 4mm and 8mm respectively. On the right, the time-averaged particle tracks are shown. There is clear separation depending on size, since the larger bubbles float straight up, whilst the smaller ones tend to follow the jet quite a bit longer. Where the interface is breached, the heavier fluid is entrained into the flux layer. At the moment this is a qualitative description, since the physics of film break-up are at present not accounted for in the model.

Finally, Figure 18 compares experimental water model frequency response curves for a case with 3cm oil covering against several simulations. One of the simulations is for a 5cm oil layer and shows significantly lower oscillation amplitudes. Two LDA points are compared, ‘x3’ close to the jet sensitive to jet oscillations and point ‘x1’ close to the oil/water interface, sensitive to interfacial waves. Although difficult to obtain point by point agreement, amplitudes are comparable in magnitude, with a significant low frequency content present, believed to be associated with the lower jet loop transport time. The simulations were limited in time due to computer cost and do not necessarily capture at this stage enough cycles of the signal at lower frequency for a meaningful FFT analysis.

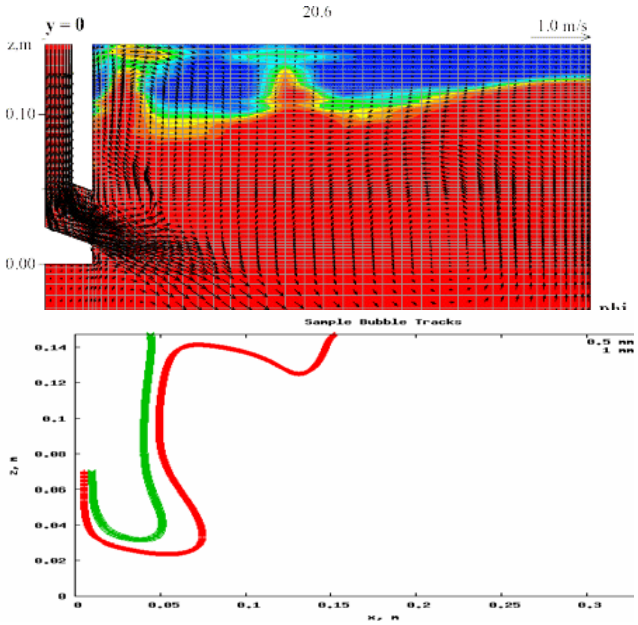

Figure 17 Time averaged bubble tracks show entrainment of the heavy fluid (red) into the lighter one (blue). In this bimodal bubble distribution, large bubbles head straight towards the surface due to buoyancy, whilst smaller bubbles tend to follow the jet further before rising.

5. Concluding Remarks

The main objective of this work has been to develop a complete fluid dynamics model of the continuous caster mould region, including the dynamic behaviour of the slag/steel interface. This model was developed by solving the source-balance transport equations for conservation of mass, momentum and turbulent kinetic energy. The model was validated against a water/oil physical model equipped with LDA velocity measurements and video recordings of interface position.

The results indicate that, mean surface profiles are generally correctly predicted with standard RANS turbulence models, but surface oscillations are damped when oil is

present. Turbulence model modifications were introduced to account, (a) for transient filtering of wave numbers in the range of interest, (b) to account for sub-grid damping due to negative density gradient stratification.

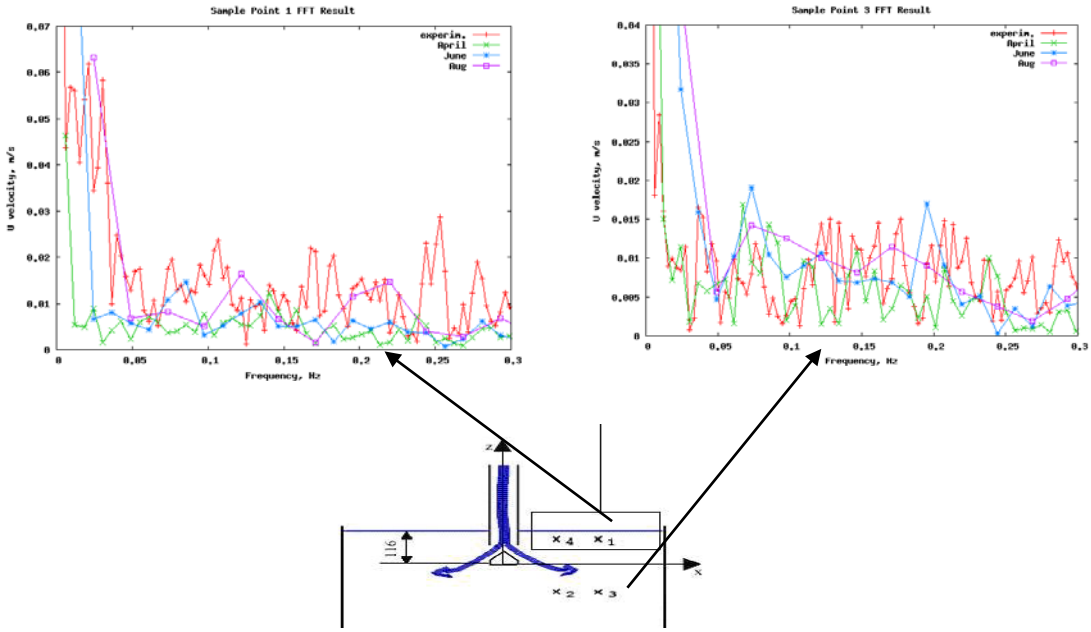

Figure 18: Frequency response at Points x1 & x3, comparing experimental results against several predictions.

Full 3D simulations take several weeks to complete using explicit VOF type techniques. A novel 'Counter-Diffusion-Method' algebraic slip model was introduced to allow implicit interface tracking calculations. Finally, oscillation amplitudes comparable to experiments were captured, including low frequency oscillations observed in the experiments. Experimental and simulation work continues.

A quasi-steady approach was used to simulate argon bubble tracks, which accounts for volume displacement and momentum exchange between gas and liquid through a mixture density approach. The argon gas has a significant influence on the SEN jets due to the added buoyancy and it also affects the behaviour of the interface. Once bubbles are allowed to penetrate the interface, they entrain liquid with them, resulting in enhanced mixing. Future work will introduce a delay mechanism, to account for the effect of interfacial tension on transit time as a function of bubble diameter.

References

[1] Thomas, B. G. and L. Zhang, "Review: Mathematical Modeling of Fluid Flow in Continuous Casting of Steel", ISIJ International, 2001, Vol. 41, No. 10, pp. 1181-1193.
[2] Domgin JF, Gardin P, "Limitation of Slag Entrainment in Tundish and Reduction of Ladle steel" Sohn Int. Symp., TMS 2006
[3] Thomas, B. G. "Modeling of the continuous casting of steel - past, present and future " Electric Furnace Conf. Proc., Vol. 59, ISS, Warrendale, PA, (Phoenix, AZ), 2001, 3-30[3] Pericleous K, Croft TN, Garding P. et al. MCWASP IX 2005
[4] Croft TN, Pericleous K, Gardin P. ECCC Birmingham, 2002
[5] Anagnostopoulos J, Bergeles G, "Three Dimensional modelling of the flow and the interface surface in a Continuous Casting Mold Model", Metallurgical and Materials Transactions B, Vol 30, pp. 1095-1105, Number 6, 1999
[6] Iguchi M, Yoshida J, Shimizu J, And Mizuno Y. "Model Study on the Entrapment of Mold Powder" , ISIJ Int. Vol. 40 (2000), No. 7, pp. 685-691
[7] PHYSICA web address: http://staffweb.cms.gre.ac.uk/~physica/
[8] Van Leer, B. (1979), "Towards the Ultimate Conservative Difference Scheme, V. A Second Order Sequel to Godunov's Method", *J. Com. Phys.*., **32**, 101–136.
[9] Stanley OJ., Ronald FP. (2002) "Level Set Methods and Dynamic Implicit Surfaces". Springer-Verlag. ISBN 0-387-95482-1.
[10] KA Pericleous, G Djambazov, H Wang "Numerical modelling of the low-superheat casting of thin-section components", MCWASP XI, Opio France, 2006
[11] Hirt CW and Nichols BD, J. Comp. Phys., 39, 201 (1981).
[12] Martin JC and Moyce WJ, "An experimental study of the collapse of liquid columns on a rigid horizontal plane", Phil.Trans.R.SOC, Vol. 244, No.882, 1952, pp.312-324.
[13] Johansen S T, Shyy W, Jiongyang W, 2Filter-Based unsteady RANS Computations", International Journal of Heat and Fluid Flow, 2003
[14] Hassan Abdulmout "The Flow Patterns in Two Immiscible Stratified Liquids Induced by Bubble Plume" Inter. Journal of Fluid Dynamics (2002), Vol. 6, Article 1
[15] Markatos, N.C. and Pericleous, K.A., "An investigation of three-dimensional fires in enclosures", Revue Generale de Thermique, 266, 1984, 67-83
[16] Cross M, Croft T N, Djambazov G and Pericleous K A, "Computational modelling of bubbles, droplets and particles in metals reduction and refining", 3rd Int. Conf. on CFD in the Minerals and Process Industries CSIRO, Melbourne, Australia 2003
[17] A.D. Gosman and E. Ioannides, "Aspects of computer-simulation of liquid-fuelled combustors", *Journal of Energy*, 7 (6) (1983), 482-490.
[18] Chevrier V, Cramb A W, "Observation and measurement of bubble separation at liquid steel-slag interfaces", Scand. J. metal. , vol. 34, n°2, pp. 89-99, 2005